On the Singularity Method of Subsonic Lifting-Surface Theory

SIEGFRIED WAGNER*
Ames Research Center, NASA, Moffett Field, Calif.

The theory presented in this paper is an extension and an improvement of the lifting-surface theories of Multhopp and Truckenbrodt for steady subsonic flow. Some of the restrictions in the application of the existing theories are removed and the accuracy of the results is improved. The range of validity of lifting-surface theory is extended to include the leading edge of the wing, and an optimal number of integration stations for spanwise integration is calculated. The positions of these integration stations are not identical with the spanwise distribution of the control points where the tangential flow condition is fulfilled. The new integration procedure, along with an accurate treatment of the singularities, allows an improved prediction of the loading of wings with complicated planforms such as double-delta and variable-sweep wings. Furthermore, a method for calculating the spanwise distribution of the leading-edge-suction force and of the induced drag is developed.

Nomenclature

A = aspect ratio, b^2/S
b = wing span, $2s$
$c(\eta)$ = local streamwise chord
$c_{d_i}(\eta)$ = coefficient of local induced drag
$c_l(\eta)$ = local lift coefficient
$c_m(\eta)$ = local pitching-moment coefficient about local quarter chord
$c_n(\eta)$ = spanwise pressure distribution functions
$c_t(\eta)$ = local leading-edge-thrust coefficient
C_{D_i} = coefficient of induced drag based on the spanwise distribution of circulation (Munk's theory), drag/$q_\infty S$
$C_{D_{ii}}$ = coefficient of induced drag based on thrust, $C_{D_{ii}} = C_L \cdot \alpha - C_T$
C_L = lift coefficient, lift/$q_\infty S$
ΔC_p = incremental pressure coefficient, $\Delta p/q_\infty$
C_T = thrust coefficient, thrust/$q_\infty S$
C_{T_M} = thrust coefficient, using Munk's theory, $C_L \cdot \alpha - C_{D_i}$
$E(k)$ = complete elliptic integral of second kind
$f_n(\eta)$ = dimensionless spanwise pressure distribution functions, $c_n(\eta)c(\eta)/2b$
$g(\xi,\eta,\eta') = \sum_{n=0}^{N} H_n(\xi,\eta,\eta')f_n(\eta')$
$h_n(X)$ = chordwise pressure distribution functions
$H_n(X,Y)$ = influence functions
k,k' = moduli of complete elliptic integrals
$K_n(\xi_p,\eta_\nu,\eta') = H_n(\xi_p,\eta_\nu,\eta_\nu) - H_n(\xi_p,\eta_\nu,\eta')$
$K(k)$ = complete elliptic integral of first kind
M = Mach number or number of spanwise control sections
M_1,M_2 = number of integrating stations for spanwise quadrature
N = $N + 1$ = number of chordwise control points
Δp = lifting pressure, $p_{lower} - p_{upper}$
q_∞ = dynamic pressure
$Q_n(\xi_p,\eta_\nu,\eta') = H_n(\xi_p,\eta_\nu,\eta' \to \eta_\nu) - H_n(\xi_p,\eta_\nu,\eta_\nu)$
R = number of integrating stations for chordwise quadrature
s = wing semispan
S = total wing area or suction force
T = thrust
U = free-stream velocity
u,v,w = perturbation velocities
x,y,x',y' = Cartesian coordinates (see Fig. 1)
X = $(x - x_{le})/c$
Y = $(y - y')/c$
α = angle of attack, rad
β = Prandtl-Glauert compressibility factor, $(1 - M^2)^{1/2}$
δ = 2δ = width of strip near control sections (see Fig. 5)
ϵ_p = $\eta_{max}' - \eta_\nu$, locations of maxima of kernel functions
θ = trigonometric variable for spanwise quadrature
Λ = leading-edge sweep angle, deg
ξ,η,ζ = Cartesian coordinates nondimensionalized with respect to $b/2$
ξ_p,η_ν = coordinates of the control points
τ = dimensionless thrust coefficient, $c_t(\eta)c(\eta)/2b$
φ = arc cot $(\beta \cdot \cot \Lambda)$
Φ_1,Φ_2 = functions representing the leading- and trailing-edge sweep

Subscripts

ac = aerodynamic center
e = experiment
le = leading edge
te = trailing edge
th = theory

Presented as Paper 69-37 at the AIAA 7th Aerospace Sciences Meeting, New York, January 20–22, 1969; submitted February 6, 1969; revision received July 2, 1969.

* National Research Council Associate. Member AIAA.

I. Introduction

THE study discussed in this paper was performed with the objective of improving the numerical solution of the singular integral equation of lifting-surface theory for steady subsonic flow.

There exist various approaches to this problem, each of them having certain advantages and disadvantages, which, however, are not discussed in this paper. This has already been done by other authors, for instance, Landahl and Stark.[1] For the present solution, the collocation method has been chosen, starting from the theories of Multhopp[2] and Truckenbrodt.[3] It is intended to remove some of the restrictions of these theories[2,3] and to change some of the numerical procedures to improve the accuracy of the results. It should be noted that both of these theories were formulated at a time when high-speed computing was at the beginning of development, and one had to compromise between the accuracy of the results and the computing effort required. Many authors[4–7] have incorporated certain improvements and modifications of the theories[2,3] by selecting more chordwise control points or changing their spanwise positions or by modifying some numerical procedures with respect to automatic computation. However, the basic methods remained unchanged, i.e., no control points are allowed at the

leading edge of the wing, and the positions of the control points (where the tangential flow condition is fulfilled) and the integrating stations are identical. But, if the spanwise gradients of the wing loading are steep or discontinuous (e.g., near the wing tips, at discontinuities in the wing planform, or near deflected flaps), a large number of integrating stations and (since they are identical with the control points) a large number of control points are required to accurately define the spanwise pressure distribution. This requires the treatment of a large number of linear equations.

Garner and Fox[8] modified Multhopp's method in such a way that the number of spanwise integration stations is a multiple of the number of spanwise control sections. But they did not optimize the distribution of integration stations. There are, of course, other methods, (e.g., Refs. 9–12), which do not share the restrictions of Multhopp-Truckenbrodt type methods. Nevertheless, all the methods mentioned so far do not allow leading-edge control points.

In the present theory, the validity of the integral equation of lifting-surface theory is extended to include the leading edge of the wing. Five chordwise control stations (including the leading and trailing edges) are used, and integration in the chordwise direction is accomplished with improved accuracy, especially near the spanwise singularities. The spanwise pressure distribution functions are approximated by Multhopp's well-known approximation polynomials. Thus, the system of integral equations is transformed into a set of linear equations for the unknown values of spanwise pressure distribution functions at a number of spanwise control sections. The remaining integrals that have to be evaluated in spanwise direction involve a singularity. To accomplish this integration with high accuracy, the wing is divided into three spanwise regions. The first region consists of a small strip in the vicinity of the control point. The second and third regions consist of the wing to the left and to the right of this strip, respectively. In the first region, which involves the singularity, the influence functions are approximated by functions that contain all the singularities. The integrals in this region can then be solved analytically. In the second and third regions, the integrals are evaluated by a Gaussian quadrature rule. In addition, an optimal number of integration stations is computed, and their positions differ completely from the distribution of control points.

Finally, a formula is derived to compute the spanwise distribution of the leading-edge-suction force and the induced drag. The results of the present theory are compared with former methods and with experiments.

II. Integral Equation of Lifting-Surface Theory for Calculating the Pressure Distribution of Wings

The present theory is based on the initial assumptions of the lifting-surface theories of Multhopp[2] and Truckenbrodt.[3] The wing is replaced by a sheet of singularities, and the strength of these singularities (which is proportional to the resultant pressure between the lower and upper surfaces of the wing) is obtained by fulfilling the tangential flow condition along the surface of the wing and the Kutta condition at the trailing edge. This leads to the following singular integral equation for the unknown pressure distribution:

$$\alpha(\xi,\eta) = -\frac{1}{8\pi} \oint_{-1}^{+1} \int_{\xi_{le}} \frac{\Delta C_p(\xi',\eta')}{(\eta-\eta')^2} \times \left\{1 + \frac{\xi-\xi'}{[(\xi-\xi')^2 + \beta^2(\eta-\eta')^2]^{1/2}}\right\} d\xi' d\eta' \quad (1)$$

This integral contains a strong singularity at $\eta \to \eta'$ and has to be defined by

$$\oint_{-1}^{+1} \frac{g(\xi,\eta,\eta')}{(\eta-\eta')^2} d\eta' = \lim_{\epsilon \to 0} \left[\int_{-1}^{\eta-\epsilon} \frac{g(\xi,\eta,\eta')}{(\eta-\eta')^2} d\eta' + \int_{\eta+\epsilon}^{+1} \frac{g(\xi,\eta,\eta')}{(\eta-\eta')^2} d\eta' - \frac{2}{\epsilon} g(\xi,\eta,\eta) \right], \quad \xi_{le} < \xi \leqq \xi_{te} \quad (2)$$

The wing geometry and the coordinate system used are illustrated in Fig. 1.

It is assumed that the pressure distribution can be represented by a linear combination of spanwise and chordwise pressure distribution functions (pressure modes):

$$\Delta C_p = \frac{2b}{c(\eta)} \sum_{n=0}^{N} h_n(\xi) f_n(\eta) \quad (3)$$

Thus, the integration of Eq. (1) in chordwise direction can be separated from the integration in spanwise direction:

$$\alpha(\xi,\eta) = -\frac{1}{2\pi} \sum_{n=0}^{N} \oint_{-1}^{+1} \frac{H_n(\xi,\eta,\eta')}{(\eta-\eta')^2} f_n(\eta') d\eta' \quad (4a)$$

$$H_n(\xi,\eta,\eta') = H_n(X,Y) = \int_0^1 h_n(X') \left\{1 + \frac{X-X'}{[(X-X')^2 + Y^2]^{1/2}}\right\} dX' \quad (4b)$$

where

$$X = [b/2c(\eta')][\xi - \xi_{le}(\eta')], \quad X' = [b/2c(\eta')][\xi' - \xi_{le}(\eta')], \quad Y = [b\beta/2c(\eta')](\eta - \eta') \quad (5)$$

Following the basic assumptions of Multhopp and Truckenbrodt, the chordwise pressure modes $h_n(\xi)$ are prescribed by utilizing the pressure distribution functions of two-dimensional thin-airfoil theory† (the arguments justifying this assumption are discussed in Ref. 13):

$$h_n(X) = \frac{1}{\pi} \left(\frac{1-X}{X}\right)^{1/2} \left[\frac{T_n(1-2X) + T_{n+1}(1-2X)}{1-X}\right], \quad n = 0,1,2,\ldots,N \quad (6a)$$

The functions T_n are Chebyshev polynomials of the first kind with the argument $1 - 2X$. The functions h_n can be handled more easily when transformed to trigonometric arguments.

$$h_n(\Psi) = \frac{2}{\pi} \frac{\cos n\Psi + \cos(n+1)\Psi}{\sin\Psi}, \quad n = 0,1,2,\ldots,N \quad (6b)$$

where

$$X' = \tfrac{1}{2}(1 - \cos\Psi) \quad (7)$$

The pressure modes h_n are illustrated in Fig. 2. It has been shown[2,3] that the spanwise pressure modes

$$c_n(\eta) = [2b/c(\eta)] f_n(\eta) \quad (8)$$

have a physical meaning when the pressure distribution functions $h_n(\xi)$ of Eqs. (6) are used. For instance, c_0 and c_1 are proportional to the local lift and local pitching moment, respectively.‡

$$c_0(\eta) = c_l(\eta) \quad (9a)$$

$$c_1(\eta) = 4c_m(\eta) \quad (9b)$$

† Usually the pressure distribution on a thin air-foil is described by

$$\Delta C_p = A_0 \cot\frac{\Psi}{2} + \sum_{n=1}^{N} A_n \sin n\Psi$$

‡ The coefficients A_n are related with the $c_n = (2b/c)f_n$ by $c_0 = (\pi/4)(2A_0 + A_1)$ and $c_n = (\pi/4)(A_{n+1} - A_n)$.

Since the chordwise pressure modes are prescribed, the integration in chordwise direction is reduced to the evaluation of the so-called influence functions $H_n(X,Y)$ in Eq. (4b), which now depend only on the geometry of the wing planform and the Mach number. Thus, the integral equation for the unknown pressure distribution $\Delta C_p(\xi,\eta)$ given in Eq. (1) is transformed into a system of integral equations for the unknown spanwise pressure modes $f_n(\eta)$, Eq. (4a).

III. Solution of the Integral Equation of Lifting-Surface Theory, Including the Leading Edge

Distribution of Control Points

Because of the high amount of computation, the tangential flow condition cannot be fulfilled along the whole surface of the wing but only at a restricted number of points, which may be called control points. In the present method, $N + 1 = 5$ chordwise control points are used at each of the $M = 15$ spanwise control sections. The coordinates of the control points are

$$X_p = [b/2c(\eta_\nu)][\xi_p(\eta_\nu) - \xi_{le}(\eta_\nu)] = p/N,\ p = 0,1,\ldots,N \tag{10a}$$

$$\eta_\nu = \cos[\pi\nu/(M+1)],\ \nu = 1,2,\ldots,M \tag{10b}$$

The reason for selecting these positions for the control points is explained in Refs. 13 and 14. It may be remarked that the spanwise control lines include the leading and trailing edges.

Integration in Chordwise Direction

It has been shown in Sec. II that the chordwise integration of the integral equation (1) is identical with the computation of the influence functions that only depend on the geometry of the wing planform and the Mach number. However, exact calculation of the influence functions is unfortunately quite laborious, because, even for the first two functions H_0 and H_1, one gets very complicated expressions involving elliptic integrals of the first, second, and third kind. For $n \geqq 2$, the analytic formulation of the influence functions becomes so difficult that one is more or less forced to look for other methods. Since the elliptic integrals have to be evaluated numerically anyhow, a convenient alternative in this case is numerical integration. Therefore, in the present method, the influence functions are computed by the following Gaussian quadrature formula (see Refs. 13 or 14):

$$H_n(X,Y) = \frac{1}{R+1}\left[q_0 + \sum_{i=1}^{R} G_{ni}q_i\right] + \begin{cases} 1, & n = 0 \\ 0, & n = 1,2,\ldots \end{cases} \tag{11a}$$

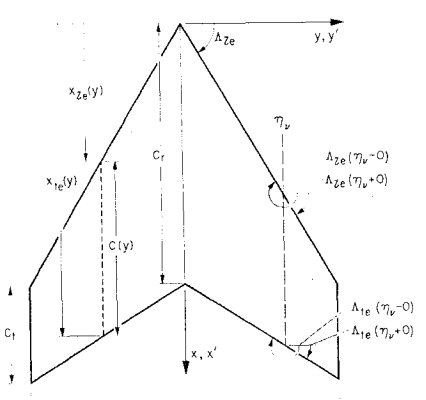

Fig. 1 Wing geometry and coordinate system.

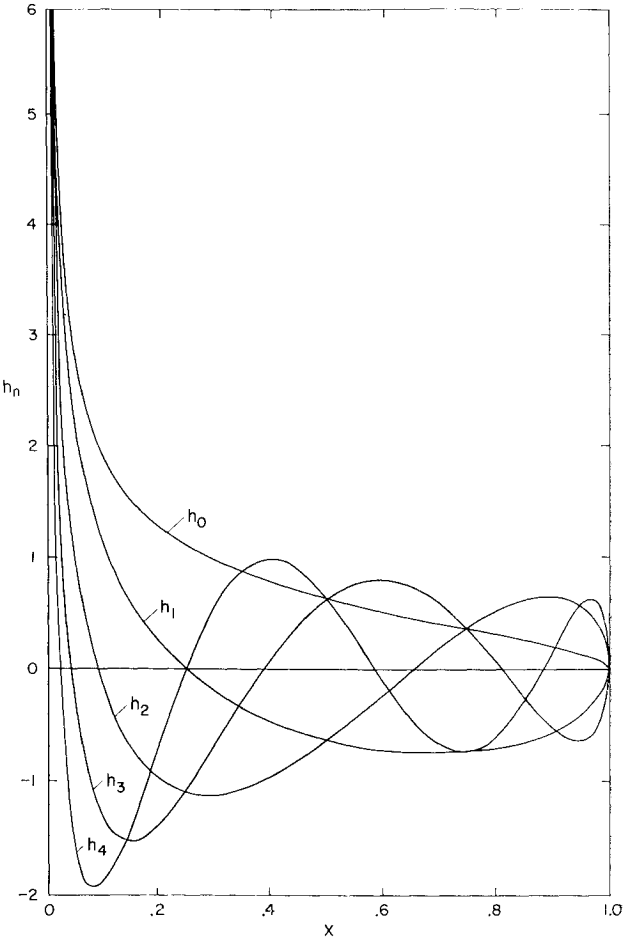

Fig. 2 Chordwise pressure distribution functions.

where

$$q_0 = X\cdot(X^2 + Y^2)^{-1/2} \tag{11b}$$

$$q_i = (2X - 1 + \cos\Psi_i)[(2X - 1 + \cos\Psi_i)^2 + 4Y^2]^{-1/2} \tag{11c}$$

$$G_{ni} = \cos n\Psi_i + \cos(n+1)\Psi_i \tag{11d}$$

$$\Psi_i = \pi\cdot i/(R+1),\ i = 1,2,\ldots,R \tag{11e}$$

If $Y = 0$, the application of Eqs. (11) requires modification. But that is unimportant since, for that case, the integrals can be solved exactly.

$$H_0(X,Y=0) = (2/\pi)(\Psi_0 + \sin\Psi_0),\ n = 0 \tag{12a}$$

$$H_n(X,Y=0) = \frac{2}{\pi}\left[\frac{\sin n\Psi_0}{n} + \frac{\sin(n+1)\Psi_0}{n+1}\right], \tag{12b}$$

$$n = 1,2,\ldots$$

$$\Psi_0 = \arccos(1 - 2X),\ 0 \leqq \Psi_0 \leqq \pi \tag{12c}$$

Furthermore, one has to notice that the integrands of the influence functions

$$I_n(X,Y,\Psi) = [\cos n\Psi + \cos(n+1)\Psi] \times \{1 + (2X - 1 + \cos\Psi)[(2X - 1 + \cos\Psi)^2 + 4Y^2]^{-1/2}\}, \tag{13}$$

$$n = 0,1,2,\ldots$$

have very steep gradients for small values of Y (i.e., near the spanwise singularities) as illustrated in Fig. 3. In these regions, the numerical computation of the influence functions has to be performed very carefully, since the accuracy of the computation, especially near the singularities, has an

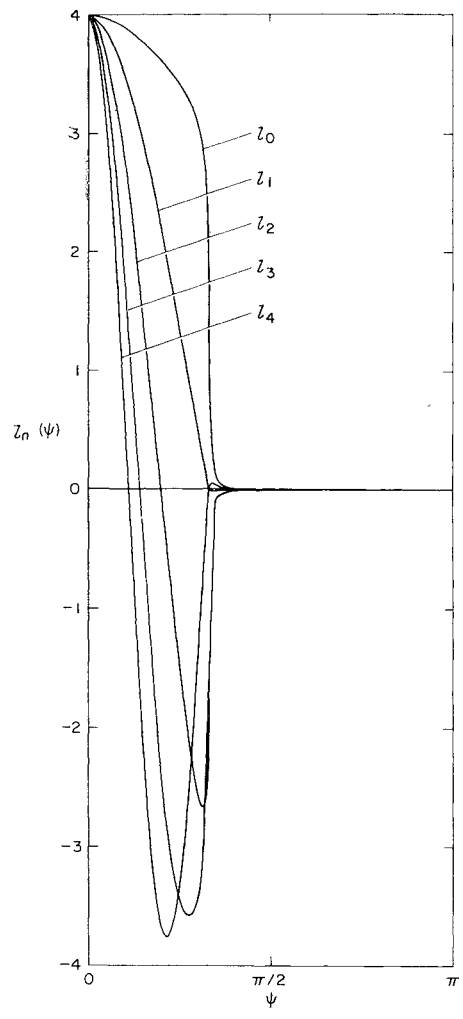

Fig. 3 Typical integrands $l_n(\psi)$ of influence functions $H_n(X,Y)$ for $X = -0.25$ and $Y = 0.01$.

important influence on the accuracy of the final solution. To accomplish best accuracy, it is recommended that the number of integration stations, R, be selected in accordance with the relationship $R = 6j - 1 (j = 1,2,\ldots)$. Extensive investigations have shown that, for instance, the relative error can be kept below 0.01% by selecting the following numbers R for different domains of Y: $0.1 \leqq Y$, $R = 29$; $0.05 \leqq Y < 0.1$, $R = 65$; $0.001 < Y < 0.05$, $R = 233$; $0.00005 \leqq Y \leqq 0.001$, $R = 329$.

Integration in Spanwise Direction

Fulfilling the tangential flow condition at the $(N + 1) \cdot M$ control points (ξ_p,η_ν), one gets the following system of integral equations for the unknown spanwise pressure modes $f_n(\eta)$, $n = 0,1,\ldots,N$ [see Eq. (4a)]:

$$\alpha(\xi_p,\eta_\nu) = -\frac{1}{2\pi} \oint_{-1}^{+1} \frac{g(\xi_p,\eta_\nu,\eta')}{(\eta_\nu - \eta')^2}\, d\eta', \qquad \nu = 1,2,\ldots,M; \quad p = 0,1,\ldots,N \tag{14a}$$

where

$$g(\xi_p,\eta_\nu,\eta') = \sum_{n=0}^{N} H_n(\xi_p,\eta_\nu,\eta') f_n(\eta') \tag{14b}$$

To solve this system of singular integral equations, one has to investigate the behavior of the function $g(\xi_p,\eta_\nu,\eta')$ in the vicinity of the control points. Therefore, the influence functions $H_n(\xi_p,\eta_\nu,\eta')$ are developed for small values of Y.

$$H_n(\xi_p,\eta_\nu,\eta' \to \eta_\nu) = H_n(\xi_p,\eta_\nu,\eta_\nu) + Q_n(\xi_p,\eta_\nu,\eta') \tag{15}$$

where

$$Q_n(\xi_p,\eta_\nu,\eta') = \Phi_1(\varphi_{le})|Y|^{1/2} + (1 + 2n + 2n^2)\Phi_2(\varphi_{le})|Y|^{3/2}, \quad p = 0 \tag{16a}$$

$$Q_n(\xi_p,\eta_\nu,\eta') = 2h_n(X_p)\tan\varphi_p Y - \frac{dh_n(X_p)}{dX'} Y^2 \ln|Y|, \quad p = 1,2,3 \tag{16b}$$

$$Q_n(\xi_p,\eta_\nu,\eta') = (-1)^n(1 + 2n)\Phi_2(\varphi_{le})|Y|^{3/2}, \quad p = 4 \tag{16c}$$

The values $H_n(\xi_p,\eta_\nu,\eta_\nu) = H_n(X_p,0)$ can be calculated by Eqs. (12). The functions $\Phi_1(\varphi)$ and $\Phi_2(\varphi)$ represent the influence of leading- and trailing-edge sweep.

$$\Phi_1(\varphi) = (8/\pi) \cdot [1/(\cos\varphi)^{1/2}][E(k) - k'K(k)]/(1 + k') \tag{17a}$$

$$\Phi_2(\varphi) = -\frac{8}{3\pi} \cdot \frac{1}{(\cos\varphi)^{3/2}} \frac{[E(k) + k'K(k)]\sin\varphi + 2k'K(k)}{1 + k'} \tag{17b}$$

$$k^2 = 1 - k'^2 = 4\cos(\pi/4 - \varphi/2)/[1 + \cos(\pi/4 - \varphi/2)]^2 \tag{17c}$$

In the above formulas, the angle φ should be the angle $\varphi_{le} = \text{arc cot}\,(\beta \cot\Lambda_{le})$ for the leading edge and $\varphi_{te} = \text{arc cot}\,(\beta \cot\Lambda_{te})$ for the trailing edge. For $p = 1,2,3$, one has to use the relation $\tan\varphi_p = [1/\beta][(1 - X_p)\tan\Lambda_{le} + X_p \tan\Lambda_{te}]$. The angles Λ_{le} and Λ_{te} are measured between the η axis and the wing edge (see Fig. 1). For the calculation of the functions $\Phi_1(\varphi)$ and $\Phi_2(\varphi)$, the angles are valid only in the interval $-(\pi/2) \leqq \varphi < (\pi/2)$. On passing from the half-plane to the right of the section η_ν to that to the left, $\Phi_1(\varphi)$ and $\Phi_2(\varphi)$ should be replaced by $\Phi_1(\pi - \varphi)$ and $\Phi_2(\pi - \varphi)$.

According to Eq. (16a), the singularity at the leading edge is of order $\frac{3}{2}$ (see also Ref. 15). Therefore, at the leading edge, Eq. (2) is no longer valid. To get the correct result, one has to evaluate integrals of the form (see also Ref. 13).

$$\lim_{\zeta \to 0} \frac{\partial}{\partial\zeta} \left[\zeta \int_{\eta_\nu - \delta}^{\eta_\nu} \frac{(\eta_\nu - \eta')^{1/2} d\eta'}{(\eta_\nu - \eta')^2 + \zeta^2} + \zeta \int_{\eta_\nu}^{\eta_\nu + \delta} \frac{(\eta' - \eta_\nu)^{1/2} d\eta'}{(\eta_\nu - \eta')^2 + \zeta^2} \right] = -4\delta^{-1/2}$$

This result indicates that the singular integrals of Eq. (4a) are also valid for the leading edge. The only, but important, difference is that they are not defined by Cauchy's principle value but by Hadamard's[16] theory of finite part integrals

$$\oint_a^y \frac{d\eta}{(y - \eta)^{i+1/2}} = \frac{(-1)^i 2^i}{2i - 1} \left(\frac{\partial}{\partial y}\right)^i \int_a^y \frac{d\eta}{(y - \eta)^{1/2}} = \frac{-2}{(2i - 1)(y - a)^{i-1/2}}, \quad i = 1,2,\ldots \tag{18}$$

where $a < y$, as shown by Mangler.[17]

There are no rigorous mathematical rules for the solution of the system of integral equations (14). Multhopp[18] developed a very efficient method for solving integral equations. He expressed the unknown function as a trigonometric interpolation polynomial and defined the integration stations in such a manner that the function values themselves, instead of the Fourier coefficients, appear as the unknowns; this amounts in fact to a linear transformation of the integral equation. Multhopp[2] and Truckenbrodt[3] do not apply the method of Ref. 18 to the unknown spanwise pressure dis-

tribution functions $f_n(\eta)$ alone, but to the functions

$$\bar{g}(\xi_p,\eta_\nu,\eta') = g(\xi_p,\eta_\nu,\eta') - \left(\frac{1-\eta'^2}{1-\eta_\nu^2}\right)^{1/2} \sum_{n=0}^{N} Q_n(\xi_p,\eta_\nu,\eta') f_n(\eta_\nu)$$

This procedure has the advantage that many matrix elements of the set of linear equations are zero. Thus, the computing effort required is reduced remarkably, and comparisons with measurements have shown that the results are satisfactory for simple planforms. The spanwise coordinates of the M control points and of the integration stations appropriate to the M-point integration rule are identical and prescribed (see Fig. 4). However, for wings with complicated planforms, such as double-delta or variable-sweep wings, a large number of spanwise integrating stations and (since they are identical with the spanwise control sections) a large number of control points are required to accurately define the spanwise pressure modes. This requires the treatment of a very large number of linear equations. Therefore, in the present theory a method is developed, where the spanwise integration stations are not identical with the spanwise control sections. First, Eqs. (14) are transformed into a more convenient form.

$$\alpha(\xi_p,\eta_\nu) = \frac{1}{2\pi} \sum_{n=0}^{N} \lim_{\epsilon\to 0} \left\{ II_n(\xi_p,\eta_\nu,\eta_\nu) \times \left[\frac{2}{\epsilon} f_n(\eta_\nu) - \fint_{-1}^{+1} \frac{f_n(\eta')d\eta'}{(\eta_\nu-\eta')^2} \right] + I_{np}(\eta_\nu) \right\}, \quad \nu = 1,2,\ldots,M \tag{19a}$$

$$I_{np}(\eta_\nu) = \fint_{-1}^{+1} \frac{K_n(\xi_p,\eta_\nu,\eta')}{(\eta_\nu-\eta')^2} f_n(\eta')d\eta', \quad p = 1,2,\ldots,N \tag{19b}$$

$$I_{np}(\eta_\nu) = \fint_{-1}^{+1} \frac{K_n(\xi_p,\eta_\nu,\eta')}{(\eta_\nu-\eta')^2} f_n(\eta')d\eta', \quad p = 0 \tag{19c}$$

where

$$K_n(\xi_p,\eta_\nu,\eta') = II_n(\xi_p,\eta_\nu,\eta_\nu) - II_n(\xi_p,\eta_\nu,\eta') \tag{20}$$

and

$$\fint_{-1}^{+1} \ldots d\eta' = \int_{-1}^{\eta_\nu-\epsilon} \ldots d\eta' + \int_{\eta_\nu+\epsilon}^{1} \ldots d\eta' \tag{21}$$

For the unknown spanwise pressure modes $f_n(\eta')$, Multhopp's well-known development of the Lagrangian interpolation formula is now introduced.

$$f_n(\theta') = \sum_{m=1}^{M} f_{nm} s_m(\theta') \tag{22a}$$

where

$$s_m(\theta') = \frac{2}{M+1} \sum_{\mu=1}^{M} \sin\mu\theta_m \sin\mu\theta' = \begin{cases} 1 & (\theta' = \theta_m) \\ \dfrac{1}{M+1} \dfrac{(-1)^{m+1}\sin\theta_m \sin(M+1)\theta'}{\cos\theta' - \cos\theta_m} & (\theta' \neq \theta_m) \end{cases} \tag{22b}$$

and

$$\theta' = \arccos\eta' \tag{22c}$$

The functions $f_{nm} = f_n(\theta_m)$ are the values of the spanwise pressure modes $f_n(\eta')$ at locations

$$\eta_m = \cos\theta_m, \quad \theta_m = \pi \cdot m/(M+1), \quad m = 1,2,\ldots,M \tag{23}$$

Using the interpolation formula (22), the first integral in Eq. (19a) can be evaluated analytically.

$$\frac{1}{2\pi} \lim_{\epsilon\to 0} \left[\frac{2}{\epsilon} f_n(\eta_\nu) - \fint_{-1}^{+1} \frac{f_n(\eta')d\eta'}{(\eta_\nu-\eta')^2} \right] = \sum_{m=1}^{M} b_{\nu m} f_{nm} \tag{24}$$

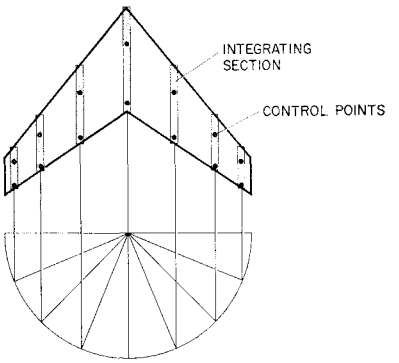

Fig. 4 Multhopp's method: location of control points and integraitng stations.

where

$$b_{\nu m} = \begin{cases} \dfrac{M+1}{4\sin\theta_\nu} & (\theta_\nu = \theta_m) \\ -\dfrac{1-(-1)^{\nu+m}}{2(M+1)} \cdot \dfrac{\sin\theta_m}{(\cos\theta_\nu - \cos\theta_m)^2} & (\theta_\nu \neq \theta_m) \end{cases} \tag{25}$$

Integrating the integrals of Eqs. (19b) and (19c), the wing is divided into three regions (Fig. 5). The first region consists of a small strip of width 2δ in the vicinity of the control point. The second and third regions consist of the wing to the left and to the right of this strip, respectively.

In the first region, which involves the singularity, the influence functions are approximated by Eq. (15), and the unknown functions $f_n(\eta')$ are replaced by $f_n(\eta_\nu)$ since $\delta > \epsilon$ is a very small positive number. Now the integrals can be evaluated analytically and with high accuracy by choosing an appropriate value for δ. Defining the coefficients

$$A_{np_{\nu\nu}} = -\frac{1}{2\pi} \fint_{\eta_\nu-\delta}^{\eta_\nu+\delta} \frac{Q_n(\xi_p,\eta_\nu\eta')}{(\eta_\nu-\eta')^2} d\eta', \quad p = 0 \tag{26a}$$

$$A_{np_{\nu\nu}} = -\frac{1}{2\pi} \lim_{\epsilon\to 0} \fint_{\eta_\nu-\delta}^{\eta_\nu+\delta} \frac{Q_n(\xi_p,\eta_\nu,\eta')}{(\eta_\nu-\eta')^2} d\eta', \quad p = 1,2,\ldots,N \tag{26b}$$

the following results are obtained for the first region $\eta_\nu - \delta \leqq \eta' \leqq \eta_\nu + \delta$:

$$A_{np_{\nu\nu}} = \frac{1}{\pi} \left[\frac{b\beta}{2c(\eta_\nu)} \right]^{1/2} \left\{ [\Phi_1(\varphi_{le}\langle\eta_\nu - 0\rangle) + \Phi_1(\varphi_{le}\langle\eta_\nu + 0\rangle)]\delta^{-1/2} - (1+2n+2n^2) \frac{b\beta}{2c(\eta_\nu)} \times [\Phi_2(\varphi_{le}\langle\eta_\nu - 0\rangle) + \Phi_2(\varphi_{le}\langle\eta_\nu + 0\rangle)]\delta^{1/2} \right\}, \quad p = 0 \tag{27a}$$

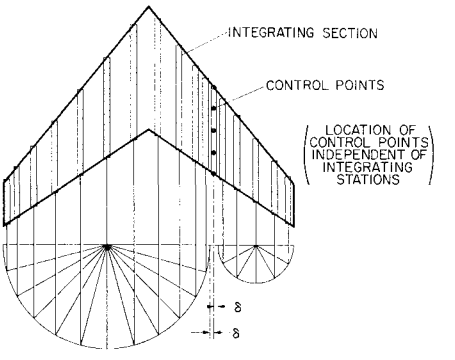

Fig. 5 Present method: spanwise distribution of integrating stations for one spanwise section of control points.

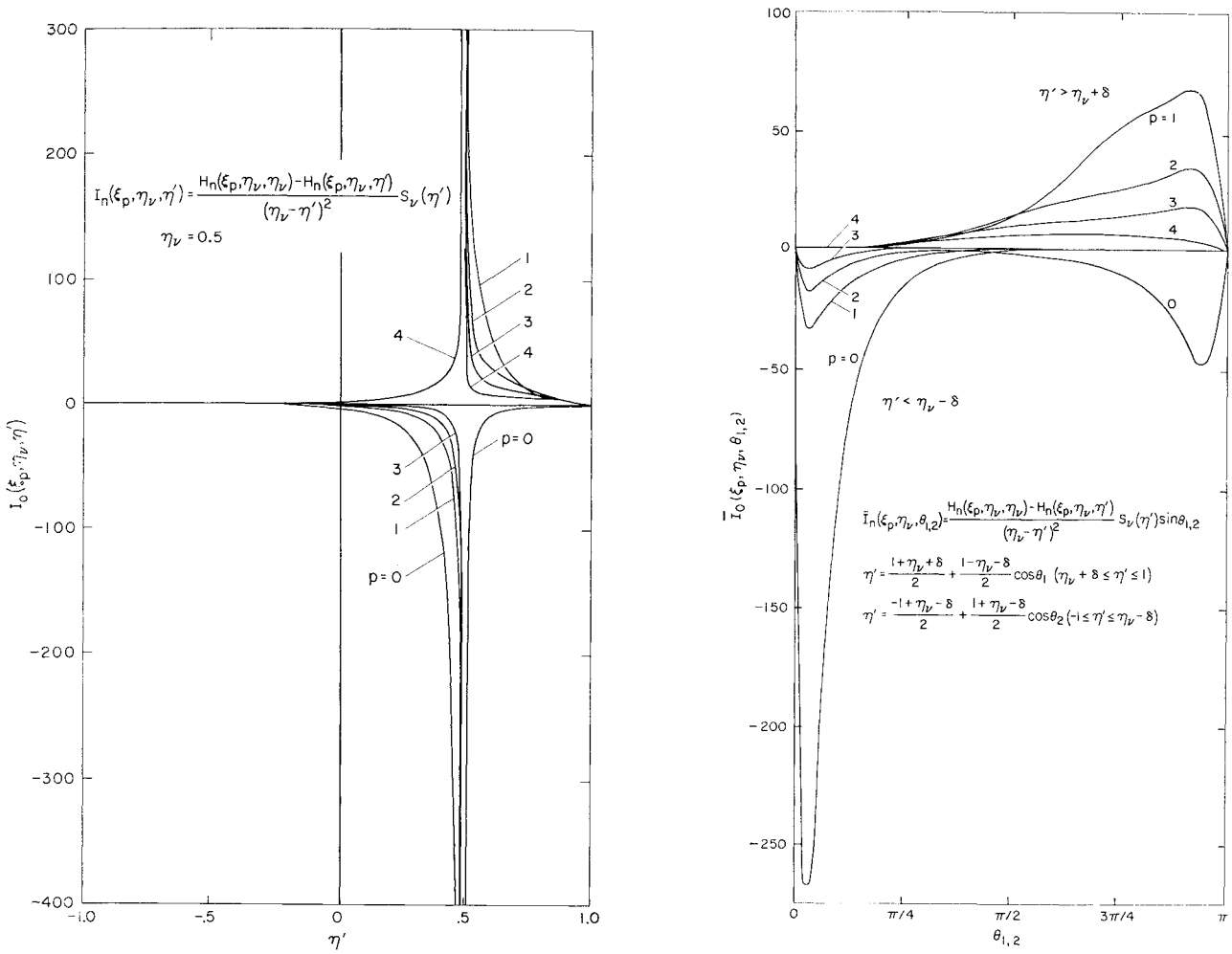

a) Typical integrands **b) Transformed integrands**

Fig. 6 Integration in spanwise direction.

$$A_{np_{\nu\nu}} = \frac{1}{\pi}\frac{dh_n(X_p)}{dX'}\left[\frac{b\beta}{2c(\eta_\nu)}\right]^2\left\{\delta\left[\ln\frac{b\delta\beta}{2c(\eta_\nu)} - 1\right]\right\}, \tag{27b}$$

$p = 1,2,3$

$$A_{np_{\nu\nu}} = \frac{(-1)^{n+1}}{\pi}(1+2n)\left[\frac{b\beta}{2c(\eta_\nu)}\right]^{3/2} \times \{\Phi_2[\varphi_{te}(\eta_\nu - 0)] + \Phi_2[\varphi_{te}(\eta_\nu + 0)]\}\delta^{1/2}, \; p = 4 \tag{27c}$$

In the second and third regions of the wing, the integrals of Eqs. (19b) and (19c) can be evaluated numerically approximating $f_n(\eta')$ by Eqs. (22). Since the integrands of the integrals are very steep near the singularity, i.e., at one end of the integration interval (Fig. 6a), the integration domains $-1 \leqq \eta' \leqq \eta_\nu - \delta$ and $\eta_\nu + \delta \leqq \eta' \leqq 1$ are transformed to an interval $0 \leqq \theta_{1,2} \leqq \pi$

$$\eta' = \eta_1 = \frac{1+\eta_\nu+\delta}{2} + \frac{1-\eta_\nu-\delta}{2}\cos\theta_1, \tag{28a}$$

$$\eta_\nu + \delta \leqq \eta_1 \leqq 1$$

$$\eta' = \eta_2 = \frac{-1+\eta_\nu-\delta}{2} + \frac{1+\eta_\nu-\delta}{2}\cos\theta_2, \tag{28b}$$

$$-1 \leqq \eta_2 \leqq \eta_\nu - \delta$$

§ For integration purposes, one has to neglect the first term of Eq. (16b) as shown in Ref. 13.

The transformed integrands are zero at both ends of the integration interval having a maximum at the end near the singularity (Fig. 6b). The integrals are now evaluated by a gaussian quadrature rule.

$$B_{np_{\nu m}} = \frac{1-\eta_\nu-\delta}{4\pi}\int_0^\pi \frac{K_n(\xi_p,\eta_\nu,\eta_1)}{(\eta_\nu-\eta_1)^2} s_m(\eta_1)\sin\theta_1 d\theta_1 = \frac{1-\eta_\nu-\delta}{4}\frac{1}{M_1+1}\sum_{i=1}^{M_1}\frac{K_n(\xi_p,\eta_\nu,\eta_i)}{(\eta_\nu-\eta_i)^2} s_m(\eta_i)\sin\theta_i \tag{29a}$$

where

$$\eta_i = \eta_1(\theta_i) \text{ and } \theta_i = \pi i/(M_1+1),\; i = 1,2,\ldots,M_1 \tag{29b}$$

$$C_{np_{\nu m}} = \frac{1+\eta_\nu-\delta}{4\pi}\int_0^\pi \frac{K_n(\xi_p,\eta_\nu,\eta_2)}{(\eta_\nu-\eta_2)^2} s_m(\eta_2)\sin\theta_2 d\theta_2 = \frac{1+\eta_\nu-\delta}{4}\frac{1}{M_2+1}\sum_{i=1}^{M_2}\frac{K_n(\xi_p,\eta_\nu,\eta_j)}{(\eta_\nu-\eta_j)^2} s_m(\eta_j)\sin\theta_j \tag{30a}$$

where

$$\eta_j = \eta_2(\theta_j) \text{ and } \theta_j = \pi j/(M_2+1),\; j = 1,2,\ldots,M_2 \tag{30b}$$

Summarizing all the results, the following set of linear equations for the $(N+1)\cdot M$ unknowns, f_{nm} is obtained.

$$a_\nu\alpha_{p\nu} = \sum_{n=0}^{N}\sum_{m=1}^{M} f_{nm}(a_{\nu m}H_{np_{\nu\nu}} + D_{np_{\nu m}}), \tag{31}$$

$$\nu = 1,2,\ldots,M;\; p = 0,1,\ldots,N$$

where

$$a_\nu = \frac{1}{b_{\nu\nu}},\ a_{\nu m} = \frac{b_{\nu m}}{b_{\nu\nu}},\ D_{np_{\nu m}} = a_\nu[\delta_{\nu m}A_{np_{\nu m}} + B_{np_{\nu m}} + C_{np_{\nu m}}]$$

$\delta_{\nu m}$ is the Kronecker symbol: $\delta_{\nu m} = 0$ for $\nu \neq m$ and $\delta_{\nu m} = 1$ for $\nu = m$. The expressions for the quantities $s_m(\eta_i)$ and $s_m(\eta_j)$ are

$$s_m(\eta_{i/j}) = \begin{cases} 1 & (\eta_{i/j} = \cos\theta_m) \\ (-1)^{m+1}\dfrac{\sin\theta_m \sin[(M+1)\arccos\eta_{i/j}]}{\eta_{i/j} - \cos\theta_m} & (\eta_{i/j} \neq \cos\theta_m) \end{cases} \quad (32)$$

The following considerations should be noted in context of the quadrature formulas (29) and (30) regarding the choice of M_1 and M_2. The integrands in Eqs. (29a) and (30a) have sharp peaks in the vicinity of η_ν, i.e., at one end of the integration interval (see Fig. 6b). To increase the accuracy, it is therefore advisable in numerical calculations to locate one integration station at the maximum of the integrand. This demand can be used to calculate M_1 and M_2. Because of the complex structure of the influence functions $H_n(\xi_p,\eta_\nu,\eta')$, it is difficult to locate the maxima of the integrands exactly. Therefore, the functions $H_n(\xi_p,\eta_\nu,\eta')$ are replaced by their approximations $H_n(\xi_p,\eta_\nu,\eta' \to \eta_\nu)$, so that we have $K_n(\xi_p,\eta_\nu,\eta' \to \eta_\nu) = -Q_n(\xi_p,\eta_\nu,\eta')$. The error evolved will not be large because the maxima are located near η_ν, and therefore, we may also assume $s_m(\eta') \approx 1$. The coordinate of the maximum is obtained from $(d/d\theta)[Q_n(\xi_p,\eta_\nu,\eta')\sin\theta/(\eta_\nu - \eta')^2] = 0$, where η' is defined by Eqs (28). The positions $\epsilon_p(\eta_\nu) = \eta_{\max}' - \eta_\nu$ for the different chordwise control stations are ($n = 0$).

$$\epsilon_0(\eta_\nu) = (1 - \eta_\nu + \delta) - [(1-\eta_\nu)^2 - \delta(1-\eta_\nu) + \delta^2]^{1/2} \quad \text{(leading edge)} \quad (33a)$$

$$\epsilon_4(\eta_\nu) = [(1-\eta_\nu)\delta]^{1/2} \quad \text{(trailing edge)} \quad (33b)$$

$$2(\epsilon_p - \delta)(1 - \eta_\nu - \epsilon_p) + [8c(\eta_\nu)/b\epsilon_p\beta]\,X_p(1-X_p) \times [(1-\eta_\nu)(\epsilon_p - 2\delta) + \epsilon_p\delta]\tan\varphi_p + \epsilon_p(1 - \eta_\nu + \delta - 2\epsilon_p)\ln[b\epsilon_p\beta/2c(\eta_\nu)] = 0, \quad p = 1,2,3 \quad (33c)$$

For $X_p = 0.25$, 0.5, and 0.75, ϵ_p has to be determined as a root of the transcendental equation (33c). After having calculated ϵ_p, the number of integration stations M_1 is obtained from

$$M_1(\xi_p,\eta_\nu) = \pi n_M \left\{\arccos\left[1 - \frac{2(\epsilon_p - \delta)}{1 - \eta_\nu - \delta}\right]\right\}^{-1} \quad (34)$$

$$p = 0,1,\ldots,N$$

Numerical investigations have shown that optimal results are achieved when the fourth integration station is located at the maximum, i.e., $n_M = 4$. It must be remembered that, sometimes at the trailing edge, the distances of the maxima from the control section are too great, so that it is inaccurate to replace the influence functions by the approximation curves. However, in these cases, the integrands

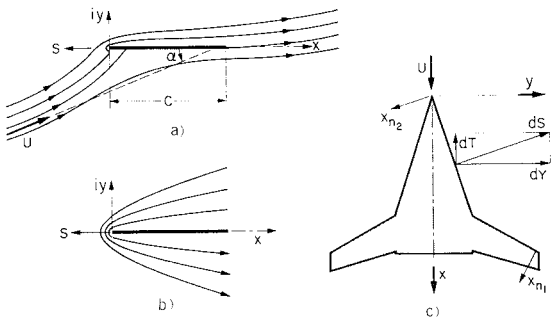

Fig. 7 Computation of suction-force distribution.

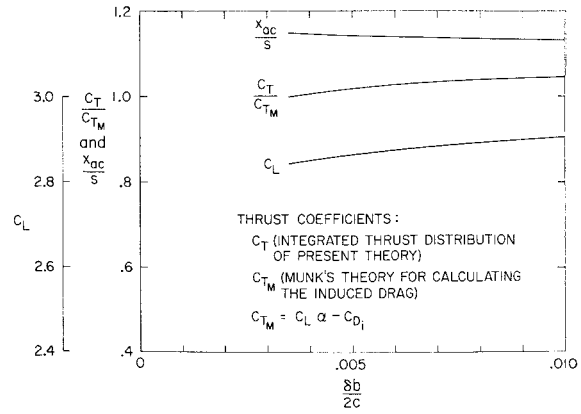

Fig. 8 Accuracy check of present method.

are very flat curves and have no steep maxima. Therefore, it is not necessary to put an integration station at the maximum, and there is also no need to change the procedure for calculating the number of integration stations since they have no influence in the results.

There is a similar formula for calculating M_2, but for a symmetric wing, $M_2(\eta_\nu) = M_1(\eta_{M+1-\nu})$. The numbers M_1 and M_2 are integers, and therefore, the results of Eq. (34) must be rounded off.

IV. Calculation of Spanwise Distribution of Induced Drag and Leading-Edge-Suction Force

In order to calculate the spanwise distribution of induced drag, one has to compute the spanwise distribution of lift and thrust, which is the component of suction force in streamwise direction. Since the flow near the leading edge of a flat plate at an angle of attack (Fig. 7a) is similar to the stream round a sharp wedge (Fig. 7b), one should be able to use results of two-dimensional potential theory. Grammel[19] showed that the suction force S at such a sharp wedge in incompressible flow is equal to $\pi\rho G^2$ if the velocity near the leading edge becomes infinite like

$$w(z \to 0) = \lim_{z\to 0} Gz^{-1/2}$$

where $z = x + iy$ and G is a real constant. This result can be transferred to the incompressible flow round a flat plate (Fig. 7a) where the velocity field can be found to be

$$w(z) = U\{\cos\alpha - i\sin\alpha[(z-c)/z]^{1/2}\}$$

The constant G is now

$$G = \lim_{z\to 0} w(z)z^{1/2} = Uc^{1/2}\sin\alpha \approx U\alpha c^{1/2},\ \alpha \ll 1$$

Thus, one obtains for the suction force, $S = \rho\pi G^2 = \pi\rho c U^2 \sin^2\alpha$. This result is identical with the exact solution. It also shows that the suction force S depends only on the nature of the velocity u. In compressible subsonic flow, one has to reduce the velocity to the incompressible case using the Prandtl-Glauert rule. The suction force obtained by this procedure has to be corrected then by the same similarity rule.

$$u = G/\beta x^{1/2} \quad (35a)$$

$$S = \pi\rho G^2/\beta \quad (35b)$$

It is assumed (see Ref. 20) that this concept can be extended to a three-dimensional wing, surmising that the suction force at a point along the leading edge depends only on the nature of the induced velocity normal to the edge at that point. The velocity u near the leading edge of a wing is

$$u(\xi \to \xi_{le},\eta) = \frac{U}{\pi}\left(\frac{2b}{c}\right)^{1/2}\sum_{n=0}^{N} f_n(\eta)\lim_{\xi\to\xi_{le}}(\xi - \xi_{le})^{-1/2}$$

	METHOD	C_L	$\frac{(C_L)_e-(C_L)_{th}}{(C_L)_e}$	$\frac{x_{ac}}{s}$	$\frac{(x_{ac})_e-(x_{ac})_{th}}{(x_{ac})_e}$
—·—	THEORY (Ref. 3)	3.153	-14.7%	1.093	9.3%
— —	THEORY (Ref. 3) EXTENDED TO 5 CHORDWISE CONTROL POINTS	3.084	-12.1%	1.103	8.5%
——	PRESENT THEORY	2.844	-3.4%	1.148	4.7%
○	EXPERIMENT (Ref. 6)	2.750	—	1.205	—

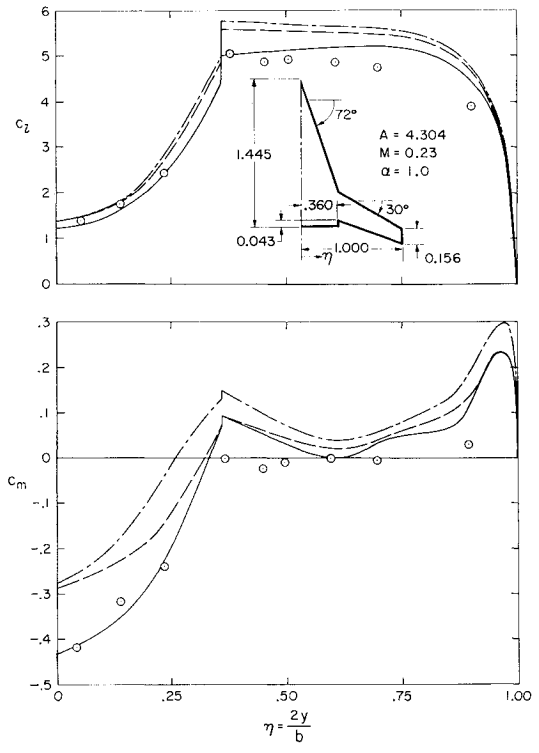

a) Spanwise lift and pitching-moment distribution

	$\frac{C_T}{C_L^2}$	$\frac{C_{T_M}}{C_L^2}$	$\frac{C_{T_M}-C_T}{C_{T_M}}$	$\frac{C_{D_i}}{C_L^2}$	$\frac{C_{Dii}}{C_L^2}$	$\frac{C_{D_i}-C_{Dii}}{C_{D_i}}$
—·—	0.330	0.242	-36.4%	0.075	-0.013	117.3%
— —	.304	.249	-22.1%	.075	.020	73.3%
——	.276	.276	0%	.075	.075	0%

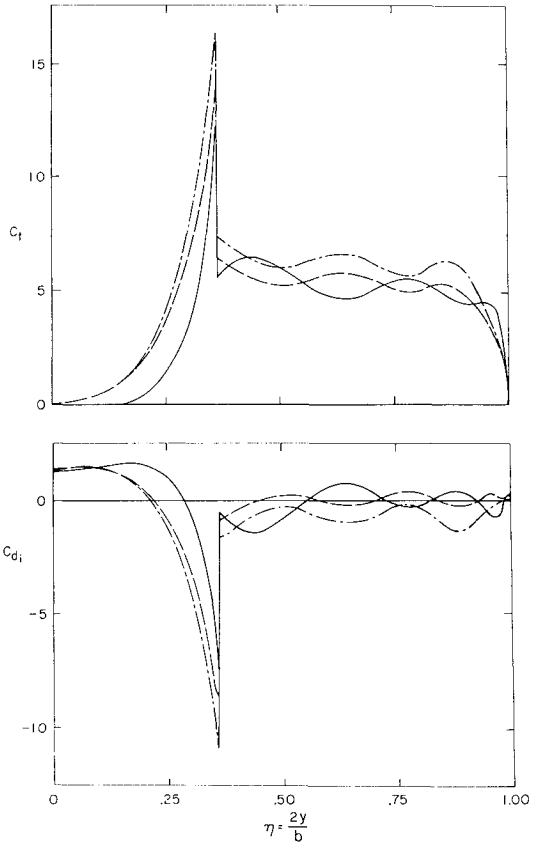

b) Spanwise distribution of leading-edge thrust and induced drag

Fig. 9 Forces and moments predicted by three theoretical methods and compared with measurements for A = 4.304 variable-sweep wing at M = 0.23.

To obtain the normal velocity, one has to evaluate

$$u_n = \frac{\partial}{\partial x_n}\int_{x_{le}}^{x} u dx = \frac{Ub}{\pi c^{1/2}}(x_n \cos\Lambda_{le})^{-1/2}\sum_{n=0}^{N} f_n(\eta) \quad (36)$$

where x_n and y_n are coordinates of a system, the axes of which are normal and parallel, respectively, to the leading edges of the wing (see Fig. 7c). To use Eqs. (35) correctly, one has to replace u by u_n and β by

$$\beta_n = [1 - (M\cos\Lambda_{le})^2]^{1/2} = \sin\Lambda_{le}(1 + \beta^2\cot^2\Lambda_{le})^{1/2} \quad (37)$$

The thrust T or the suction force S is now obtained from

$$dS/dy_n = dT/dy = (\pi\rho/\beta_n)G_n^2 \quad (38)$$

where

$$G_n = \beta_n \lim_{x_n\to 0} u_n x_n^{1/2} = \frac{Ub\beta_n}{\pi(c\cos\Lambda_{le})^{1/2}}\sum_{n=0}^{N} f_n(\eta) \quad (39)$$

Putting Eq. (39) into (38), one finally gets

$$\frac{dT}{d\eta} = \frac{\rho\beta_n U^2 b^3}{2c\pi\cos\Lambda_{le}}\left[\sum_{n=0}^{N} f_n(\eta)\right]^2$$

or

$$C_T = A\int_{-1}^{+1}\tau(\eta)d\eta \quad (40)$$

where

$$\tau(\eta) = \frac{c_l(\eta)c(\eta)}{2b} = \frac{b(1+\beta^2\cot^2\Lambda_{le})^{1/2}}{\pi c(\eta)\cot\Lambda_{le}}\left[\sum_{n=0}^{N} f_n(\eta)\right] \quad (41)$$

After $c_l(\eta)$ has been calculated, the spanwise distribution of the induced-drag coefficient is simply obtained from

$$c_{d_i}(\eta) = c_l(\eta)\alpha - c_l(\eta) \quad (42)$$

The coefficient of the total induced drag can now be computed in two different ways. One can either use the coefficient of the total thrust obtained by integrating the thrust distribution

$$C_{D_{ii}} = C_L\cdot\alpha - C_T \quad (43)$$

or Munk's theory[21]:

$$C_{D_i} = A\int_{-1}^{+1} f_0\alpha_i d\eta = \frac{\pi}{4}A\left[\sum_{\nu=1}^{M} f_{0\nu}^2 + 2\sum_{\nu=1,3,\ldots}^{M}\sum_{m=2,4,\ldots}^{M} a_{\nu m}f_{0\nu}f_{0m}\right] \quad (44)$$

The comparison of C_{D_i} and $C_{D_{ii}}$ or C_T and $C_{T_M} = C_L\alpha - C_{D_i}$ is also a sensitive indicator for the numerical accuracy of a lifting-surface theory. In the present theory, it is used to determine the best value of $Y_{\min} = \delta b/2c(\eta)$.

There is an optimal value for $Y_{\min}$. If $Y_{\min}$ is getting larger and larger the assumption that $f_n(\eta')$ is equal to $f_n(\eta_\nu)$ = const within $\eta_\nu - \delta \leq \eta' \leq \eta_\nu + \delta$ becomes increasingly less accurate. If $Y_{\min}$ is getting smaller, the errors in the numerical integration procedure increase since the peaks of the integrands near the singular point (see Fig. 6b) maximize. Figure 8 shows that the accuracy of the present theory is very good and that C_T/C_{T_M}, C_L, and x_{ac}/s do not change too much with $Y_{\min}$.

V. Results

To investigate the accuracy of the present theory, the loading has been calculated for a variable-sweep wing as illustrated in Fig. 9a. The results are compared with measurements¶ of Ref. 6 and with Truckenbrodt's theory,[3] which uses two chordwise control points. To get a better idea of the improvement of the present theory due to the new quadrature procedures, Truckenbrodt's method was extended to five chordwise control points located at the same positions as the present method. Therefore, the extended Truckenbrodt method now involves the treatment of the leading-edge singularity, also. In Fig. 9a, the spanwise distributions of lift and pitching moment computed by several theories are compared with measurements. At the inboard panel, the theoretical lift distributions are in good agreement with the measurement, whereas at the outboard panel, the deviations become larger. The differences in the results between the present theory and the measurements are the lowest and acceptable. The over-all lift of the present theory differs from the measurements by 3.4%. A remarkable improvement by the present theory is obtained for the inboard pitching-moment distribution, which agrees well with measurements, whereas at the tips one would wish a better improvement.

Since the pitching-moment distribution is also used to calculate the suction-force distribution, the inaccuray of the original and extended Truckenbrodt methods** in predicting the pitching moment is also reflected in the distribution of the leading-edge thrust and of the induced drag (Fig. 9b). These methods predict a higher suction-force distribution than the present method, especially at the inboard panel, which causes a distribution of low induced drag. The total drag $C_{D_{ii}}$, computed by integrating the distribution, is even negative in Truckenbrodt's original theory. Therefore, the comparison of total thrust C_T obtained by integrating the distribution and C_{T_M} calculated with Munk's theory do not agree very well in both the original and extended Truckenbrodt theory, where the errors are 36.4 and 22.1%, respectively. Lamar[6] showed that Multhopp's theory[2] can be improved by choosing an optimal combination of chordwise and spanwise control sections. This should also be valid for Truckenbrodt's theory.[3] However, the number of matrix elements usually increases rapidly.

VI. Applications

The theory discussed in this paper can be applied to low cambered wings with arbitrary polygonal planforms, including highly swept wings, so long as the results of a linear theory are meaningful. The idea for computing an optimal number and distribution of spanwise integration stations might also be useful for other theories, e.g., Ref. 9. The calculated distribution of the induced drag and leading-edge-suction force could be used to locate appropriate devices for control of flow separation at the leading edge of wings and to get minimum induced drag for a given wing.

VII Conclusions

The lifting-surface theory at steady subsonic flow has been extended to include the leading edge of wings. Five chordwise control points have been distributed equidistantly along the chord, including the leading and trailing edges. The numerical integration procedures both in chordwise and spanwise directions used in the described theory, along with an accurate treatment of the singularity, have improved the accuracy of the results. There has also been derived a formula for calculating the spanwise distribution of leading-edge-suction force and induced drag. The present theory has been applied to compute the loading of a variable-sweep wing. The comparison with measurements and the original and extended Truckenbrodt methods has shown that the spanwise distribution of lift, pitching moment, induced drag, and leading-edge-suction force can be computed more accurately by the present method.

¶ The measurements were made at an angle of attack α = 3.14°. In Fig. 9a, the experimental results are extrapolated linearly to α = 1.0 rad.

** The suction-force distributions of the existing theories were computed by the present method using the load distributions that were predicted by the existing theories.

References

[1] Landahl, M. T. and Stark, V. J. E., "Numerical Lifting-Surface Theory—Problems and Progress," AIAA Paper 68-72, New York, 1968; also *AIAA Journal*, Vol. 6, No. 11, Nov. 1968, pp. 2049–2060.

[2] Multhopp, H., "Methods for Calculating the Lift Distribution of Wings (Subsonic Lifting-Surface Theory)," R and M 2884, 1955, Aeronautical Research Council.

[3] Truckenbrodt, E., "Tragflaechentheorie bei inkompressibler Stroemung," *Wissenschaftliche Gesellschaft für Luftfahrt, Jahrbuch*, 1953, pp. 40–65.

[4] Van Spiegel, E. and Wouters, J. G., "Modification of Multhopp's Lifting-Surface Theory with a View to Automatic Computation," NRL-TN W.2, June 1962, Natational Lucht-Ruimtevaartlab., Amsterdam.

[5] Van de Vooren, A. I., "Some Modifications to Lifting-Surface Theory," *Journal of Engineering Mathematics*, Vol. 1, No. 2, 1967, pp. 87–101.

[6] Lamar, J. E., "A Modified Multhopp Approach for Predicting Lifting Pressures and Camber Shape for Composite Planforms in Subsonic Flow," TN-D 4427, 1968, NASA.

[7] Niemz, W., "Ergaenzungen zur Tragflaechentheorie bei inkompressibler Stroemung von E. Truckenbrodt," *Wissenschaftliche Gesellschaft für Luftfahrt, Jahrbuch*, 1965, pp. 130–133.

[8] Garner, H. C. and Fox, D. A., "Algol 60 Programme for Multhopp's Low-Frequency Subsonic Lifting-Surface Theory," R and M 3517, 1966, Aeronautical Research Council.

[9] Watkins, C. E., Woolston, D. S., and Cunningham, H. G., "A Systematic Kernel Function Procedure for Determining Aerodynamic Forces on Oscillating or Steady Finite Wings at Subsonic Speeds," Rept. R-48, 1959, NASA.

[10] Hsu, P. T., "Some Recent Developments in the Flutter Analysis of Low-Aspect-Ratio Wings," *Proceedings of the National Specialists Meeting on Dynamics and Aeroelasticity*, 1958, pp. 7–26.

[11] Woodward, F. A., "A Unified Approach to the Analysis and Design of Wing-Body Combinations at Subsonic and Supersonic Speeds," AIAA Paper 68-55, New York, 1968; also *Journal of Aircraft*, Vol. 5, No. 6, Nov.–Dec., 1968, pp. 528–534.

[12] Albano, E. and Rodden, W. P., "A Doublet Lattice Method for Calculating Lift Distributions on Oscillating Surfaces in Subsonic Flow," AIAA Paper 68-73, New York, 1968; also *AIAA Journal*, Vol. 7, No. 2. Feb. 1969, pp. 279–285.

[13] Wagner, S., "Beitrag zum Singularitaetenverfahren der Tragflaechentheorie bei inkompressibler Stroemung," Ph.D. thesis, Technical University, Munich, Jan. 4, 1967.

[14] Wagner, S., "Beitrag zum Singularitaetenverfahren der Tragflaechentheorie bei inkompressibler Stroemung," *Ingenieur-Archiv*, Vol. 36, Heft 6, 1968, pp. 403–420 (summary version of Ref. 13).

[15] Jordan, P. F., "Remarks on Applied Subsonic Lifting Surface Theory," *Wissenschaftliche Gesellschaft für Luft-und Raumfahrt Jahrbuch* 1967, pp. 192–210.

[16] Hadamard, J., *Lectures on Cauchy's Problem in Linear Par-*

tial Differential Equations, Yale University Press, New Haven, Conn., 1923.

[17] Mangler, K. W., "Improper Integrals in Theoretical Aerodynamics," Rept. Aero 2424, C.P. No. 94, June 1951, Royal Aircraft Establishment.

[18] Multhopp, H., "Die Berechnung der Auftriebsverteilung von Tragfluegeln," *Luftf-Forschung,* Vol. 15, 1938, pp. 153–169.

[19] Grammel, R., *Die Hydrodynamischen Grundlagen des Fluges,* Vieweg und Sohn, Braunschweig, 1917.

[20] Heaslet, M. A. and Lomax, H., "Supersonic and Transonic Small Perturbation Theory, Section D of General Theory of High Speed Aerodynamics," *High Speed Aerodynamics and Jet Propulsion,* edited by W. R. Sears, Vol. VI, Princeton University Press, Princeton, N.J., 1954, pp. 122–344.

[21] Munk, M. M., "The Minimum Induced Drag of Aerofoils," Rept. 121, 1921, NASA.

NOV.-DEC. 1969 J. AIRCRAFT VOL. 6, NO. 6

Peripheral Jets: Effect of Exit Geometry

ANDREW LOWENSTEIN,* PAUL BERRY,† AND ROBERT E. DUFFY‡
Rensselaer Polytechnic Institute, Troy, N. Y.

This investigation was designed to examine the effects of various geometric parameters of the exit on the lift of a peripheral jet device. The variables considered were: the operating height, the curtain thickness, the base extension beyond the curtain, and the shape of this base extension. Because of the large number of variables involved, a statistical method of data gathering was used. Recorded lampblack and kerosene streakline patterns and measured pressure distributions on the base of the model and on the ground plane revealed three distinct flow patterns in the vicinity of the exit depending on whether the curtain, as a result of its expansion due to mixing, left an open, a partially sealed, or a completely sealed gap between the base extension and the ground. The first occurrence of this sealing phenomenon was found to depend on the geometric parameters involved and to mark the point where the measured lift began to deviate appreciably from that predicted by the existing theories.

Nomenclature

A_g = augmentation ratio (integrated pressure on base and nose extension/jet momentum flux)
C = length of base
h = height of base above ground
$\dot{M}$ = mass flow flux from slot
N = base extension or overhang
p = static pressure (base or ground)
P_b = base static pressure
p_t = total pressure in reservoir
RN = Reynolds number based on nozzle exit conditions = $\rho_j V_j t/\mu$
t = thickness of nozzle slot
x = coordinate distance measured from inboard end of base
θ = inclination angle of nozzle measured from vertical

1. Introduction

THE peripheral-jet ground-support system is one of a variety of devices that have shown a good potential for lifting heavy loads at moderate ground clearances. The primary feature which distinguishes the peripheral-jet from other modes of fluid suspension is a jet curtain of fluid that exits from a nozzle-slot arrangement around the periphery of the base and is directed towards the ground. The deflection of this jet curtain by the ground sets up a pressure differential across the curtain. The pressure differential, in turn, acting on the base generates a lifting force.

A substantial number of theoretical and experimental studies have been conducted in an attempt to analyze the behavior of peripheral-jet support systems.[1–4] In all the studies of which the authors are aware, the nozzle and slot arrangement is always located on the outer periphery. However, it is not inconceivable to envision a ground-support system that employs a jet curtain that is located at a substantial distance inboard of the actual periphery of the device. As a matter of fact, due to stability and control problems, there are some current thoughts along this same line with regard to a support system for the tracked air-cushion vehicle (TACV).

The goal of this report is to present the results of a systematic experimental investigation that was directed to a determination of the operational performance of jet-curtain type ground-support systems that have a moderate amount of base extension or overhang outboard of the nozzle slot.

Previous researchers have established that there are a very large number of design parameters that influence the performance of peripheral-jet support systems. After considering both the magnitude of the problem and the limitations imposed on the authors by the test facilities available, the parameters and magnitudes chosen are shown in Table 1. Further, these parameters are in ratios comparable to those presently anticipated on the series of tracked air-cushion vehicles currently under development in this country.

2. Test Apparatus

Tests were conducted on a two-dimensional peripheral-jet device designed and constructed by Sandberg.[5] Slight modifications to the nozzle geometry of this device were made to provide for an adjustable slot width. In addition, extra

Received January 24, 1969; revision received May 1, 1969. This research was supported by the National Science Foundation under Grant GK-618.

* Undergraduate Student, Senior, Aeronautical Engineering and Astronautics.

† Undergraduate Student, Junior, Aeronautical Engineering and Astronautics.

‡ Associate Professor of Aeronautical Engineering and Chairman, Aeronautical Engineering and Astronautics Curriculum. Member AIAA.